Final Draft
of the original manuscript:

Huber, N.; Richert, C.:
Comment to "Skeletonization-based beam finite element models for stochastic bicontinuous materials: Application to simulations of nanoporous gold" by C. Soyarslan et al. [J. Mater. Res. 33(20), 3371 (2018)].
In: Journal of Materials Research. Vol. 35 (2020) 20, 2831 - 2834.
First published online by Cambridge University Press: 07.10.2020

https://dx.doi.org/10.1557/jmr.2020.257

Comment to „Skeletonization-based beam finite element models for stochastic bicontinuous materials: Application to simulations of nanoporous gold“ by C. Soyarslan et al. [J. Mater. Res. 33(20), 3371 (2018)]

Norbert Huber[1,2*], Claudia Richert[1]

[1]Institute of Materials Research, Materials Mechanics, Helmholtz-Zentrum Geesthacht, Geesthacht, Germany

[2]Institute of Materials Physics and Technology, Hamburg University of Technology, Hamburg, Germany

[*]*Corresponding author: norbert.huber@hzg.de*

Abstract

Soyarslan et al. [J. Mater. Res. 33(20), 3371 (2018)] proposed a beam-FE model for the computation of effective elastic properties of nanoporous materials, where the ligament diameter along the skeleton is determined with the biggest sphere algorithm. Although this algorithm is often used in literature, it is known that it systematically overestimates the diameter in network structures. Thus, the need for further stiffening of the junction zones as proposed by the authors is in contradiction to the literature. Furthermore, the factor 40 appears to be one order of magnitude too high. We show that the 3D microstructures generated from random Gaussian fields contain features that are violating the assumption of circular cross-sections and, therefore, cannot be captured by the biggest sphere algorithm. Consequently, the authors required an unphysically high value of 40 to compensate this hidden effect.

Keywords: microstructure, modeling, elastic properties

1. Introduction

Modelling and Finite Element (FE) simulation of nanoporous metals using beam-FE models allows predicting the elastic-plastic mechanical properties of complex randomized 3D structures with high computational efficiency [1, 2]. An important aspect is the representation of the junction region such that the effect of the nodal mass is correctly represented in the predicted mechanical response [2]. Significant work has been invested into the microstructure generation [1, 3, 4], skeletonization [4, 5, 6, 7], topological and geometrical analysis [4, 5, 6, 7] and investigation of the structure-property-relationship of nanoporous gold via FE modeling [4, 5, 6, 8]. A combination of these approaches is presented in [7] in form of a skeleton FE beam model. Unexpectedly, although no nodal correction has been implemented, this FE beam model overpredicted the mechanical properties of the FE solid model, provided in Refs. [5, 6]. The reason is that the biggest sphere algorithm [9] systematically overpredicts the ligament thickness when there is a strong variation in the radius along the ligament axis [7]. Consequently, the implementation of a nodal correction/junction zone strategy would lead to even larger overpredictions for which the attention turned to methods for improving the

thickness determination [10] followed by a careful bottom-up development of a nodal correction for various ligament shapes [11].

Parallel to this path, Soyarslan et al. developed a voxel-FE model for computing the macroscopic mechanical properties of a leveled-Gaussian random field model of nanoporous gold [8] and derived a relationship between the scaled Young's modulus and the phase volume fraction. In their follow-up paper [12] (received 10 May 2018) they reproduce the results previously published in [8]. Soyarslan et al. cited [13] (available online 26 March 2018) as the relevant reference for an "efficient FE beam-based modelling approach relying on skeletonization". However, Ref. [13] is a review paper, where the description of the "approach" is limited to a few sentences (page 367, last paragraph) without any details about modeling and validation of the individual steps and without further references for details. Instead, in the caption of Fig. 47(c) of [13], the reader is referred to [12]; the second reference provided there is limited to image processing, skeletonization, and topology analysis of bone. Therefore, Ref. [12] represents the original paper that establishes the approach mentioned above. With this commentary, we show that this approach does not work and, furthermore, we explain why.

In [7] (published: 19 April 2018) and referenced in Ref. [12], the thickness algorithm has been raised as a particular problem. It is clearly pointed out in the conclusions of [7] that this algorithm leads to an overestimation in the ligament diameter that causes a considerable overstiffening of the FE beam model, which even exceeds the stiffness of a FE solid model of correct geometry. Although Soyarslan et al. referenced this paper in [12], they used the biggest sphere algorithm and, surprisingly, introduced a further stiffening in the junction zone by a factor of 40 for achieving an agreement with results of the voxel-FE model. It is striking, that this obvious contradiction to the findings reported in [7] was unaddressed by the authors despite having referenced [7].

In what follows, we will shed light on the reason for the discrepancies of [12] with the insights from [2, 7]. For supporting our results with the necessary background information and details of the computation, we have published two additional papers. Reference [11] investigates the nodal correction for beam-FE models with variable ligament shape discussed in Section 2. Reference [10] (see Supplementary Material) contains the details of the image processing and modeling techniques that are used in Section 3.

2. Junction zone strategy

Soyarslan et al. [12] proposed a "stiffness intensity factor", ω, for calibrating the stiffening of the junctions. They tuned ω by fitting the macroscopic Young's modulus to the data published in [8] over a large range of phase volume fractions from $\phi_B = 0.2$ to 0.5, delivering a value of $\omega = 40$. It should be mentioned that a nodal correction was already available for elastic-plastic deformation of nanoporous gold in Ref. [2] and a comparison of Fig. 2 and Sect. 2.2 of [2] with Fig. 6(b) and Sect. B of [12] reveals many similarities. It is shown in [2] that for example at a

phase volume fraction ϕ_B =0.3 a comparably small increase in the element radius of 25% together with a 3.5-fold increase of the Young's modulus of the elements within the junction volume perfectly reproduces the mechanical properties of the corresponding FE solid model. Furthermore, the individual ligament geometry must be considered for providing a meaningful nodal correction over a larger range of phase volume fractions. This is confirmed in [11] for more general ligament shapes. Furthermore, it is shown in [11] that the junction zone strategy presented in [12] is a special case of the nodal correction proposed in [2], such that the two methods can be quantitatively compared.

According to Soyarslan et al. [12], "a stiffness factor of 40 gives a reasonable approximation for the Young's modulus for the phase volume fractions $0.20 < \Phi_B < 0.50$". This implies that the factor $\omega = 40$ applies to every junction, independent of the ligament shape and aspect ratio, whereas it is shown in [11] that this value systematically overpredicts the correct macroscopic Young's modulus by minimum +15% and up to +180%. In average, the value of ω should be around 3.7, i.e. more than a factor 10 lower and, as expected, the precise value depends on the individual ligament shape [11]. Evidently, the beam-FE model presented by Soyarslan et al. contains a source of compliance, which was compensated by making a large fraction of the model (the junction zones) nearly rigid. For examples of the extension of the junction zones for various ligament geometries see Fig. 2 in [11].

3. Circularity of cross-sections

Soyarslan et al. introduce the section *Local thickness distribution* in their work as follows [12]: "A complete geometrical description of the domain with beam FEs having circular cross sections is not possible without identification of the radii of the cross sections". As the local thickness distributions presented in Fig. 4 of [12] do not show any details of the features, we followed the approach for the generation of periodic microstructures and FE models as described in [8] and [12]. We were able to reproduce the macroscopic Young's modulus data presented in FIG. 9(a) of [12] for both types of models within about 10 percent accuracy and visualized structural details with OVITO [14]. Figure 1 compares the geometries of both models for a low phase volume fraction of $\phi_B = 0.2$. The surfaces of the voxel-FE model and the beam-FE model are represented by the golden (left) and light blue surface (right), respectively. In region (A), the thickness of the beam-FE model exceeds the size of the voxel model, confirming the overestimation by the biggest sphere algorithm reported in [7, 10]. This increases the stiffness of the model. However, as can be seen from the regions (B) and (C), a significant amount of volume around junctions and ligaments is not represented by the beam-FE model. This counteracts the known effect of stiffness increase (A) due to two mechanisms that cause a considerable loss of stiffness. Gusset plate-like masses (B) connecting two ligaments close to junctions are eroded by the skeletonization and are not captured by circular ligaments. Furthermore, ligaments with non-circular cross-sections (C) are reduced in their thickness to

their minor radius. Both effects substantially soften the beam-FE model compared to the voxel-FE model.

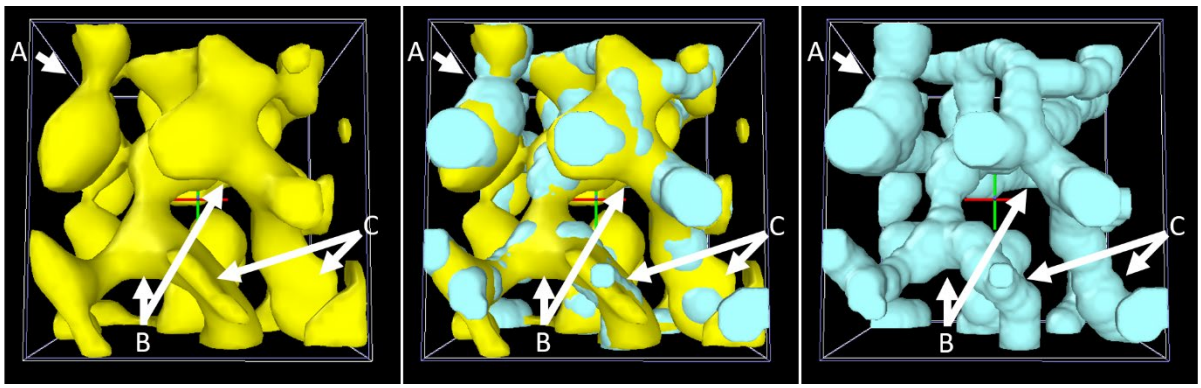

Figure 1: Surface of the voxel-FE model (left, yellow) and beam-FE model (right, light blue) for $\phi_B = 0.2$. The box size is 32x32x32 voxel positioned inside the 128x128x128 voxel RVE. The superposition of both structures is shown in the middle.

Similarly, Figure 2 compares the geometries for a phase volume fraction of $\phi_B = 0.4$. From the mass in the top right corner (B, red framed) it can be seen that the effect of stiffening by thick gusset plates is more pronounced. Several junctions and ligaments are merged in a massive block of material. Evidently, a beam-FE model is unable to capture such volumes and considerably underestimates the true size of the junctions (blue dashed circles). Consequently, the calibration of the stiffness intensity factor by Soyarslan et al. [12] via a fit of the macroscopic stiffness to the data of the voxel-FE model [8] accounts only for an unknown part of the volume of the junctions and the ligaments and, therefore, leads to an unphysically high value of $\omega = 40$ (for the proposed value see Conclusions of [12]).

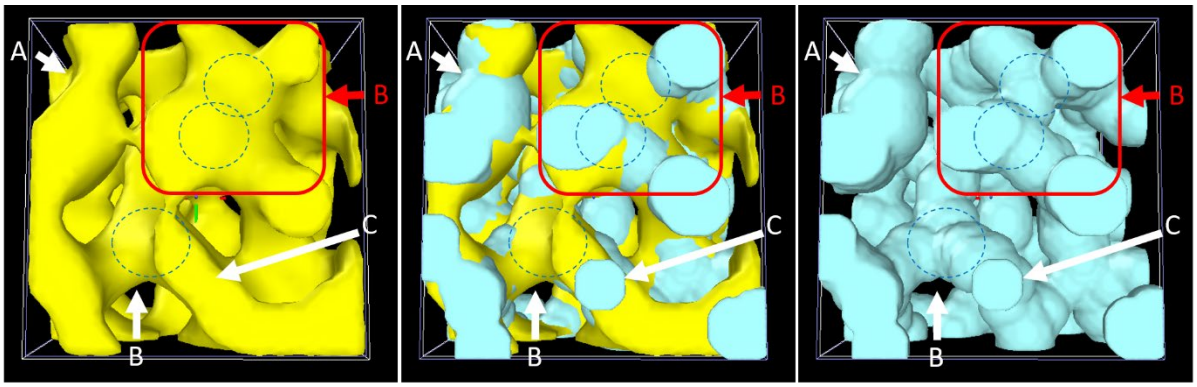

Figure 2: Surface of the voxel-FE model (left, yellow) and beam-FE model (right, light blue) for $\phi_B = 0.4$. The box size is 32x32x32 voxel positioned inside the 128x128x128 voxel RVE. The superposition of both structures is shown in the middle.

4. Conclusions

The approach presented in [12] relies on the assumption that the features of the microstructure have a circular cross section. We could show that the microstructures generated from random Gaussian fields [3, 8] considerably violate this assumption. With increasing phase volume fraction, the microstructure is massively stiffened by gusset plates, connecting neighboring ligaments. Furthermore, non-circular cross-sections are reduced to their minor size and, as a result, the load-bearing mass is only partially included in the beam-FE model. This excessively softens the mechanical response of the beam-FE model relative to the original voxel model and leads to an unphysically high value of $\omega = 40$. The reason for this is that this parameter is determined exclusively via a global fit to the macroscopic stiffness of the voxel-FE model [8], without considering the details of the individual shapes of ligaments and nodes.

Methodology

The method for the generation of the voxel-FE models shown on the left side of Figures 1 and 2 is described in [3, 8]. The surface of the structure is visualized using OVITO [14] by importing the coordinates of the FE-nodes of the voxel-FE model. After construction of the surface mesh, the particles (FE nodes) are switched off. The method for the generation of the beam-FE models shown on the right side of Figures 1 and 2 is described in [7, 10]. The volume occupied by the cylindrical beam-FE elements is filled with particles using the scan approach described in the Supplementary Material of [10], Sect. 3 Tomography of FEM beam models. After importing the particles into OVITO [14], the surface mesh is constructed and the particles are switched off. The superposition of both structures in the middle of Figures 1 and 2 follows the same procedure for both models using the import option “Add to scene”.

Acknowledgements

This work is funded by the Deutsche Forschungsgemeinschaft (DFG, German Research Foundation) – Projektnummer 192346071 – SFB 986 ‘‘Tailor-Made Multi-Scale Materials Systems: M^3”, project B4. J. Weissmüller is acknowledged for making the Mathematica script available published in [3] that allowed for reproducing the 3D microstructures. E.T. Lilleodden is acknowledged for discussions and editing of the manuscript.

References

[1] N. Huber, R. Viswanath, N. Mameka, J. Markmann and J. Weißmüller: Scaling laws of nanoporous metals under uniaxial compression. *Acta Mat.* **67**, 252-265 (2014).

[2] J. Jiao and N. Huber: Effect of nodal mass on macroscopic mechanical properties of nanoporous metals. *Int. J. Mech. Sci.* **134**, 234-243 (2017).

[3] B.-N. Ngô, A. Stukowski, N. Mameka, J. Markmann, K. Albe and J. Weissmüller: Anomalous compliance and early yielding of nanoporous gold. *Acta Mat.* **93**, 144-155 (2015).

[4] K. Mangipudi, E. Epler and C. Volkert: Topology-dependent scaling laws for the stiffness and strength of nanoporous gold. *Acta Mat.* **119**, 115-122 (2016).

[5] K. Hu, M. Ziehmer, K. Wang and E. Lilleodden: Nanoporous gold: 3D structural analyses of representative volumes and their implications on scaling relations of mechanical behaviour. *Phil. Mag.* **96**, 3322-3335 (2016).

[6] K. Hu: Micromechanical and Three–Dimensional Microstructural Characterization of Nanoporous Gold–Epoxy Composites. *PhD Thesis,* Hamburg University of Technology (TUHH), 2017.

[7] C. Richert and N. Huber: Skeletonization, Geometrical Analysis and Finite Element Modeling of Nanoporous Gold Based on 3D Tomography Data. *Metals* **8**, 282 (2018).

[8] S. Soyarslan, S. Bargmann, M. Pradas and J. Weissmüller: 3D stochastic bicontinuous microstructures: generation, topology and elasticity. *Acta Mat.* **149**, 326-340 (2018).

[9] T. Hildebrand and P. Rüegsegger: A new method for the model-independent assessment of thickness in three-dimensional images. *J. Microsc.* **185**, 67–75 (1997).

[10] C. Richert, A. Odermatt and N. Huber: Computation of thickness and mechanical properties of interconnected structures: Accuracy, deviations and approaches for correction. *Front. Mat.* **6**, 352 (2019).

[11] A. Odermatt, C. Richert and N. Huber: Prediction of elastic-plastic deformation of nanoporous metals by FEM beam modeling: A bottom-up approach from ligaments to real microstructures. *Mater. Sci. Eng. A* **791**, 139700 (2020).

[12] C. Soyarslan, H. Argeso and S. Bargmann: Skeletonization-based beam finite element models for stochastic bicontinuous materials: Application to simulations of nanoporous gold. *J. Mater. Res.* **33**, 3371-3382 (2018).

[13] S. Bargmann, B. Klusemann, J. Markmann, J. Schnabel, K. S. C. Schneider and J. Wilmers: Generation of 3D representative volume elements for heterogeneous materials: A review. *Prog. Mater. Sci.* **96**, 322-384 (2018).

[14] A. Stukowski: Visualization and analysis of atomistic simulation data with OVITO – the Open Visualization Tool. *Modelling Simul. Mater. Sci. Eng.* **18**, 015012 (2010).